Molecular Systems Biology 4; Article number 232; doi:10.1038/msb.2008.69
Citation: ***Molecular Systems Biology*** **4:232**

www.molecularsystemsbiology.com

molecular systems biology

Analysis of pairwise cell interactions using an integrated dielectrophoretic-microfluidic system

Zhizhong Yin[1], David Noren[1], C Joanne Wang, Rob Hang and Andre Levchenko*

Department of Biomedical Engineering, Johns Hopkins University, Baltimore, MD, USA
[1] These authors contributed equally to this work.
* Corresponding author. Department of Biomedical Engineering, Johns Hopkins University, 208c Clark Hall, 3400 N. Charles Street, Baltimore, MD 21218, USA. Tel.: +410 516 5584; Fax: +410 516 6240; E-mail: alev@jhu.edu

Received 29.4.08; accepted 30.10.08

Blood vessel formation, during either normal vascular reconstruction or pathogenic tumour formation, relies upon highly organized cell–cell interactions. Isolating the function of any particular component of this cell–cell communication is often difficult, given the vast complexity of communication networks in multicellular systems. One way to address this problem is to analyse cell–cell communication on the most elementary scale—cell pairs. Here, we describe an integrated dielectrophoretic (DEP)-microfluidic device allowing for such analysis. Single cancer and endothelial cells (ECs) and cell pairs were patterned using DEP force and cultured within a minimally stressful microfluidic channel network. Controlling both the initial cell positions and extracellular environment, we investigated cell motility in homo- and heterotypic cell pairs under diverse conditions. We found that secreted collagen IV and soluble vascular endothelial growth factor have considerable guidance effect on ECs at the level of two interacting cells. Cell interaction rules extracted from the experiments of cell pairs were used to mathematically predict branching patterns characteristic of developing multicellular blood vessels. This integrative analysis method can be extended to other systems involving complex multicellular interactions.
Molecular Systems Biology 16 December 2008; doi:10.1038/msb.2008.69
Subject Categories: simulation and data analysis; signal transduction
Keywords: angiogenesis; dielectrophoresis; endothelium; microfluidics; modelling

Introduction

Cell–cell interactions leading to tissue development and remodeling frequently involve a small number of cells. This raises an important question of whether the information obtained *ex vivo* on the cell population level, that is, on the basis of averaged measurements of hundreds or even millions of cells, is relevant to understanding many of the physiological and pathophysiological processes. Although potentially more pertinent information could be obtained from single cell level analyses, the corresponding experiments under the usual cell culture conditions are often hard to interpret due to variable initial population states and difficulties in dealing with poorly controlled cell distributions. Therefore, the development of tools allowing an increased degree of control of cell localization and the microenvironment holds great promise for extending our knowledge of a plethora of cell signalling events.

Current microfabrication technologies offer a convenient means to precisely control cell–cell and cell–ECM (extracellular matrix) interactions (El-Ali *et al*, 2006). For instance, single cells and cell pairs have been precisely patterned to study the effect of cell–cell contact on cell proliferation (Nelson and Chen, 2002, 2003) and the effects of the size and shape of ECM islands on cell fate (Chen *et al*, 1997). Controlled cell patterning on larger scales has been achieved by differential chemical treatment of the cell adhesion substratum (Kane *et al*, 1999; Irimia and Karlsson, 2003; Suh *et al*, 2004; Veiseh *et al*, 2004) or by using properties of laminar flow (Takayama *et al*, 1999; Khademhosseini *et al*, 2004).

Dielectrophoretic (DEP) force provides a particularly flexible and robust means for precise cell manipulation and patterning (Wang *et al*, 1997). When cells in a medium are exposed to an electric field, both the cells and the surrounding medium become electrically polarized. If the electric field is not uniform, the force acting on the part of the cell exposed to a stronger field intensity is expected to be greater than the force acting on the remainder of the cell. The unbalanced forces can drive the cell towards the maximum (positive DEP) or minimum (negative DEP) of the electric field depending on

the properties of the cell and the surrounding medium. Both positive and negative DEP force can be used to manipulate cells (Voldman *et al*, 2001; Nelson and Chen, 2003; Grey *et al*, 2004; Lin *et al*, 2006). For instance, thousands of single cells in a single microfabricated device could be precisely patterned using an electrode array generating positive DEP force on the basis of 'points-to-lid' geometry (Gray *et al*, 2004).

Microfabricated devices can be used to precisely define an extracellular chemical microenvironment with high temporal and spatial resolution (El-Ali *et al*, 2006; Melin and Quake, 2007). For example, taking advantage of the fact that flows in microchannel networks are laminar, one can generate a precisely defined chemical gradient and temperature steps for cell stimulation (Lucchetta *et al*, 2005; Weibel and Whitesides, 2006; Paliwal *et al*, 2007). Unfortunately, active cell patterning is rarely combined with the continuous medium control afforded by the microfabricated devices, limiting one's ability to precisely set both the initial experimental conditions and the cell microenvironment in the ensuing experimentation.

One research area of cell biology that can especially benefit from the simultaneous control of the initial cell positions and cell medium during experimentation is the analysis of endothelial cell (EC) biology in the context of formation of new blood vessels. The corresponding processes of angiogenesis and vasculogenesis are among the most heavily investigated due to their importance in development, tissue repair and tumourigenesis. Among many factors regulating angio- and vasculogenesis, vascular endothelial growth factor (VEGF) and proteins of the ECM appear to have especially prominent functions (Ferrara, 2004; Adams and Alitalo, 2007). Although the VEGF family includes many members, for convenience, the initially identified VEGF (VEGF-A) is still frequently referred to simply as VEGF (the convention also followed in this study). VEGF binds to several receptors: VEGFR-1, -2, -3 and neuropilin. Binding of VEGF to VEGFR-2 promotes survival and migration of ECs and secretion of matrix metalloproteinases (MMPs), and mediates the permeability of blood vessels (Matsumoto and Claesson-Welsh, 2001). Disruption of VEGF-mediated signal transduction can lead to the arrest of angiogenesis, making VEGF inhibitors promising candidates for cancer therapy (Ferrara, 2004; Herbst and Sandler, 2004). ECM can also contribute to the formation of new vessels by controlling cell adhesion, as ECs are highly anchorage dependent (Folkman, 2007). Cell interaction with the ECM appears to be highly regulated, exemplified by differential integrin expression in sprouting versus quiescent ECs (Hanahan and Weinberg, 2000).

Numerous mathematical models have been proposed to describe blood vessel formation, particularly in the area of tumour angiogenesis (Mantzaris *et al*, 2004). These models can be placed into two categories as either being continuum (Gamba *et al*, 2003; Serini *et al*, 2003; Di Talia *et al*, 2006) or discrete mathematical descriptions. Although both types of simulations have been successful in describing aspects of tumour angiogenesis, discrete models have the advantage of illustrating how simple cell interactions and behaviours can lead to complex vascular structures.

Earlier models that incorporated individual cell behaviour described vascular sprout formation by considering the biased random walk of the leading cell at the tip of a forming vessel (Stokes and Lauffenburger, 1991; Anderson and Chaplain, 1998). Initiation of new sprouts was based on the assumption that the branching probability increased as the sprout approached the tumour. More recent models describe both tip and stalk cells as discrete entities using the concept of the cellular Pott's model (Glazier and Graner, 1993). The first such study was largely focused on exploring the function of cell shape and cell contact in the formation of vascular networks (Merks and Glazier, 2006; Merks *et al*, 2006). In a more recent study, the cellular Pott's model was applied to tumour angiogenesis to examine a more comprehensive list of factors, including chemotaxis to growth factors, cell proliferation and interactions with the ECM (Bauer *et al*, 2007). However, in that study, the predicted branching patterns were a function of the imposed heterogeneity in the density of ECM and growth factor concentration.

In this report, we present a novel device combining the DEP and microfluidic flow-based control of single cell-scale experiments. We use this device to explore the details of pairwise EC–EC and EC–tumor cell interactions. We show that, on the scale of single ECs or EC–EC pairs, cell migration speed and migration patterns may be strongly affected by secreted collagen and VEGF. Further, we extract a few simple cell–cell interaction rules from the experiments. We use these rules to build a model for the evaluation of whether the secretion of insoluble and soluble cues, such as collagen and VEGF, on the level of relatively few cells might constitute a sufficient mechanism for the development of vascular branching patterns.

Results

Experimental system

The main design feature of the described microfluidic device is an array of electrodes allowing for the use of positive DEP force for cell patterning through generation of well-defined electric field maxima. The array is composed of pairs of sharply triangular indium–tin–oxide (ITO) electrodes facing each other at a distance of less than 40 μm. FEMLAB (now as COMSOL) simulations of the resultant electric field (Figure 1B) were conducted to verify that the electric field would be sharply focused around the tips of the triangular electrodes. We optimized the fabrication process to produce tips smaller than the average size of a cell ($\sim$10 μm); thus, when positive DEP force is applied, single cells are pulled down from suspension and positioned at each tip. In this manner, cell pairs were placed at controlled distances (Figure 1C). In contrast, designs with tip diameters larger than the size of a cell often resulted in positioning of multiple cells at each tip. This design feature may be exploited for other types of multicellular studies.

The ITO electrode array was reversibly integrated with a PDMS microfluidic device. This allowed for the precise regulation of the soluble microenvironment and the alteration of the cell medium composition with minimum perturbation. Although a number of fluidic layouts can be integrated with our ITO electrode array, the specific arrangement of the channels in the fluidic layer presented in this study followed

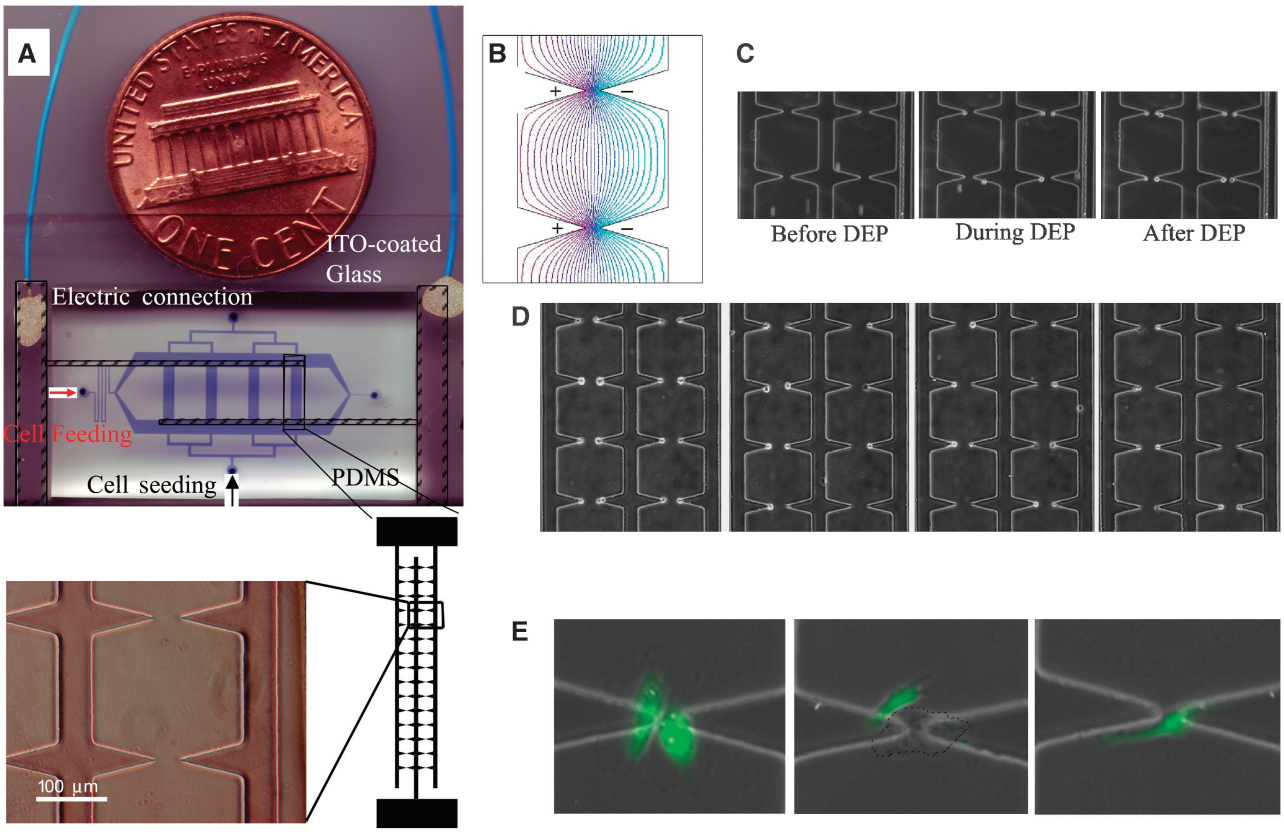

Figure 1 The dielectrophoretic (DEP)-microfluidic device and the cell patterning process. (**A**) The DEP-microfluidic device. The PDMS chip with channel network (shown in blue) is bonded to glass substrate with ITO electrodes (shown in close-up pictures, scale bar=100 μm). The ITO connection bars leading to the electrodes are outlined. (**B**) Femlab simulation of the electric field in the space separating the electrodes, showing convergence of the electric field at the electrode tips, the property used for cell capture. (**C**) Cell patterning process by positive DEP force (see Supplementary Movie 1). (**D**) A partial view of four columns of patterned cells from each of the four channels in (A). (**E**) Patterned HUVEC–HUVEC pair, HUVEC–A549 pair and a single HUVEC cell in the device after 4 h of culturing in the complete medium. The A549 cell is manually outlined.

the H-junction design described previously (Paliwal *et al*, 2007). As shown extensively in our previous work, this design can prevent active flow through the cell-containing areas and allows for the efficient diffusive transport of nutrients. An experiment with Alexa Fluor 594 dye confirmed that the media in the cell-culturing channels can be completely exchanged by diffusion within an hour (Supplementary Figure 4). This property can allow for continuous delivery and exchange of media and minimize the disturbance to the cells as they attach following the DEP-based patterning. In addition, various conditions can be quickly imposed on the single cell culture without causing potentially harmful shear stress. The ability to decouple shear stress from stimulant delivery makes this microfluidic design particularly suitable for studying vascular biology, as shear stress itself is known to alter EC behaviour. Additionally, culturing of cells in this device might better approximate actual *in vivo* conditions by limiting the cell and matrix free space above and beside cells. As the distance between the cell adhesion substratum and the test chamber 'ceiling' was 50 μm, the accumulation of secreted autocrine and paracrine factors are enhanced compared with conventional culture conditions where the depth of the medium overlaying cells is on the scale of millimetres.

We tested the device performance by patterning immortalized human umbilical vein cells (henceforth referred to as HUVEC for simplicity) constitutively expressing eGFP (Freedman and Folkman, 2004) and A549 human lung cancer cells. As expected, single cells were successfully captured at approximately 77% of the electrode tips and excess cells were washed away (Figure 1C and D). Cells were captured at electrodes in various combinations: HUVEC–HUVEC, A549–A549, HUVEC–A549 pairs and single HUVEC and A549 cells (Figure 1E), which was easy to confirm as only HUVEC cells carried eGFP. When equal proportions of A549 and HUVEC cells were introduced into the device, approximately 50% of the cell pairs were homotypic and 50% were heterotypic. Both HUVEC and A549 cells were found to adhere, move and proliferate well in the complete HUVEC culture medium or its modifications described below.

Motility of single cells and cells in homotypic and heterotypic cell pairs

Following the initial cell spreading in HUVEC culture media, we imaged the motility of live cells diffusively fed by the 'complete' (10% fetal bovine serum (FBS)) or the 'starvation' (0.5% FBS) HUVEC culture media for 17 h (this medium is expected to have reduced concentrations of growth factors, including VEGF). Upon preliminary examination of the cell

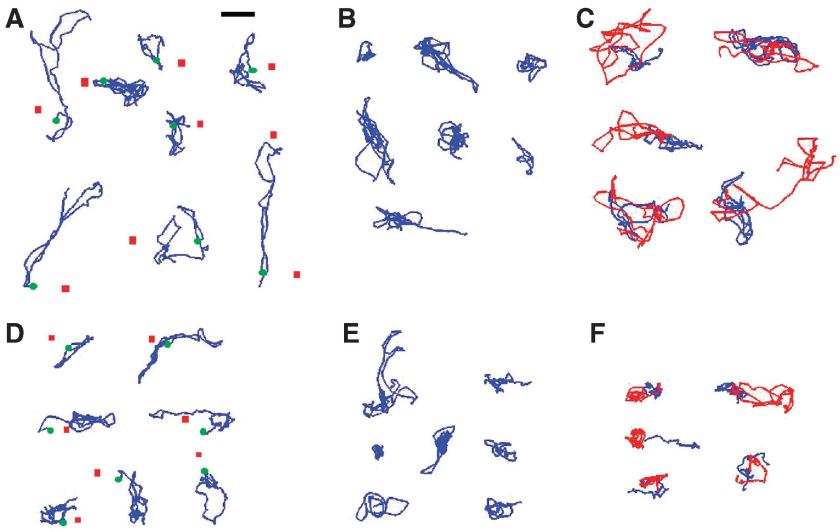

Figure 2 Sample trajectories of HUVECs incubated in different continuously replenished media for 17 h. Cells were provided with complete HUVEC culture medium, (**A**–**C**) or starvation medium, (**D**–**F**). Trajectories of cells in HUVEC–A549 pairs (A, D), single HUVECs (B, E) or cells in HUVEC–HUVEC pairs (C, F) are juxtaposed for comparison, The red and green dots represent the starting location of A549 and HUVEC cells, respectively. Scale bar=50 μm.

trajectories in HUVEC–A549 pairs (Figure 2A and D), we found that A549 cells, although viable, well-spread and constantly exhibiting transient extension of membrane projections, showed very limited motility and remained essentially stationary over the duration of the experiment. HUVEC cells, on the other hand, underwent more extensive cell movements with serum-dependent qualitative differences. In the complete medium, cell movements could be roughly grouped into two classes: (1) highly localized movement in the immediate vicinity (often with cell–cell contact) of the cancer cell and (2) extensive 'tours' of up to 200 μm away, sometimes being into close vicinity of a single cancer cell located at the adjacent electrode pair. Virtually without exception, these 'touring' cells were able to accurately retrace their paths and return back to the original locations near the cancer cell partners. The 'touring' cell behaviour was present, but much less extensive and less frequent in the starvation medium, with cells nevertheless moving vigorously around the cancer cell partners.

We next contrasted this behaviour with movement of single HUVEC cells without a cell partner or cells in HUVEC–HUVEC pairs. We found that single HUVEC cells underwent apparently random movement in both types of media, with trajectories spanning larger distances in the complete media (Figure 2B and E). Trajectories of cells in HUVEC–HUVEC pairs were similar to trajectories of single HUVECs, although cells in pairs were rarely separated by larger than a single cell diameter over the course of the experiment (Figure 2C and F). The asymmetrical nature of cell trajectories in A549–HUVEC pairs was further evidenced by higher directionality (anisotropy of the trajectory as a whole, see Materials and methods) of cell locomotion compared with single HUVEC cells or cells in HUVEC–HUVEC pairs (Figure 4E). For example, with starvation medium, the directionality for HUVECs in A549–HUVEC pairs is 3.4 ± 0.44, in comparison with 2.2 ± 0.27 (P=0.05, standard T-test) and 2.5 ± 0.66 (P=0.33, standard t-test) for single HUVEC cells and cells in HUVEC–HUVEC pairs, respectively, with the difference not statistically significant in the latter case. Of note, A549 cells can secrete VEGF, especially in response to hypoxia/hyperoxia (Shenberger *et al*, 2007). The increase of the directionality for HUVEC in A549–HUVEC pairs might therefore arise from the VEGF gradient around A549 cells.

Effect of VEGF inhibitor on motility of single cells and cell pairs

To further explore the nature of the differences among cell movement trajectories in different cell pairings, we explored whether VEGF signalling (Figure 3), previously implicated in cancer-EC interactions leading to angiogenesis, might be a controlling factor. Inhibition of VEGF-mediated receptor activation did not significantly affect cell movement in A459–HUVEC pairs but, surprisingly, had a dramatic effect on the movement of single HUVEC cells and cells in HUVEC–HUVEC pairs (5 μM of the VEGF inhibitor CBO-P11 in starvation media was supplied through the side channels throughout the experiment). In particular, the directionality of cell movement increased from 2.2 ± 0.27 to 4.3 ± 0.57 for single HUVECs (P=0.01, standard T-test) and from 2.5 ± 0.66 to 6.1 ± 0.97 for cells in HUVEC pairs (P=0.006, standard t-test), with trajectories becoming straighter and cells retracing their paths more frequently and precisely (Figure 4D). Moreover, movements of cells in HUVEC pairs became more correlated, with cells synchronizing their back-and-forth movement in apparent oscillations (Figure 3D). To verify the effect of VEGF on cell migration, we also performed a similar experiment with the anti-VEGFR 2 antibody (MAB3572). We found that addition of 250 ng/ml of the antibody into the starvation medium altered the directionality of the cell trajectories in a manner very similar to the effect of the VEGF inhibitor (Supplementary Figure 5).

The influence of VEGF on ECs can be pleiotropic. In particular, it has been implicated as a mitogen, chemoattractant,

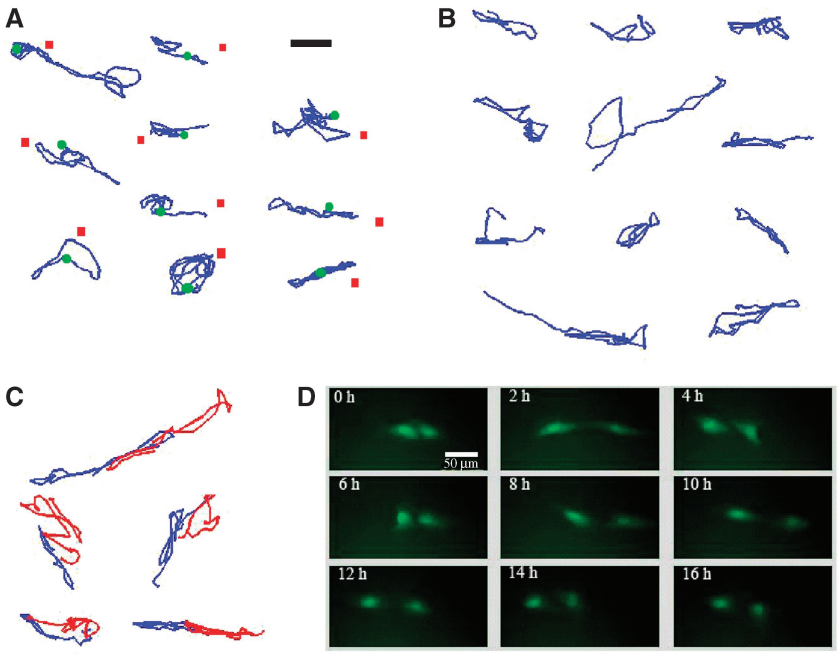

Figure 3 The effect of inhibition of VEGF signalling. (A–C) Sample trajectories of HUVECs during a 17 h time course in the presence of a VEGF inhibitor in starvation medium. (**A**) Trajectories of HUVECs in HUVEC–A549 pairs. The red and green dots represent the starting location of A549 and HUVEC cells, respectively. (**B**) Trajectories of single HUVECs. (**C**) Trajectories of HUVECs in HUVEC–HUVEC pairs. (**D**) Time lapse imaging of a HUVEC–HUVEC pair illustrating oscillatory change in the distance between cells (Supplementary Movie 3). Scale bar=50 μm.

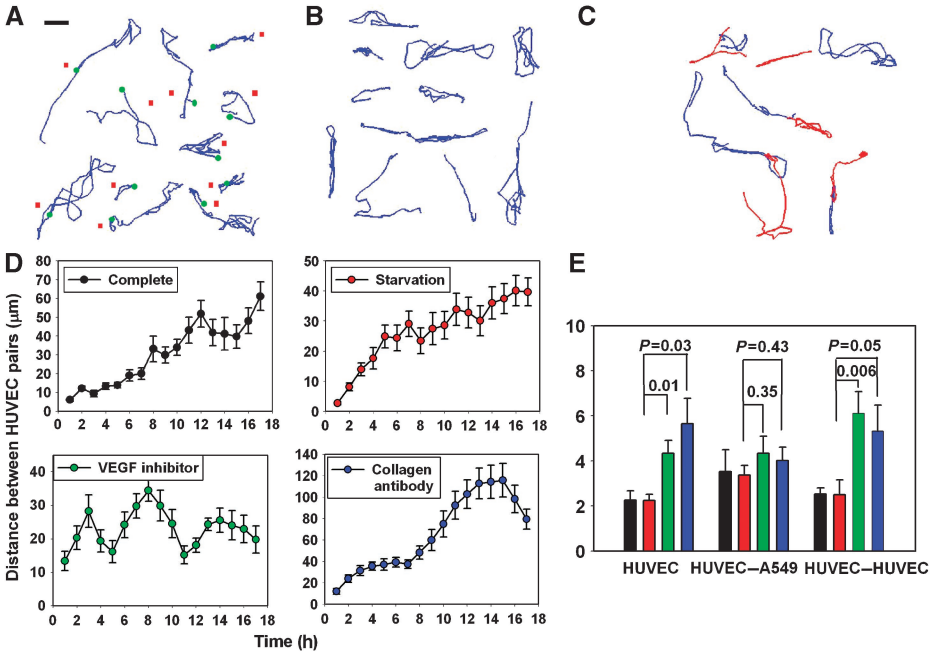

Figure 4 The effect of blocking cell–ECM interaction. (**A**–**C**) Trajectories of HUVECs in HUVEC–A549 pair, single HUVEC and HUVEC–HUVEC pairs, respectively, during a 17 h time course in the presence of an anti-collagen IV antibody in starvation medium. (**D**) Change in distance between HUVECs in HUVEC–HUVEC pairs over the same time course. Distance between cells was measured as the distance between their centroids determined using the GFP fluorescence images, with the distance at time 0 h taken to be 0. Error bar represents s.e.m. (n=5 pairs in all cases). (**E**) Directionality of HUVEC trajectories for cells incubated in the complete HUVEC culture medium (black), starvation medium (red), starvation medium supplemented with VEGF inhibitor (green), starvation medium supplemented with anti-collgen IV antibody (blue). P-values shown are obtained from the t-test.

an inducer of secretion of MMPs (Folkman, 2007) or even a survival factor (Lee *et al*, 2007). The last two functions might have important implications for cell locomotion and, thus, affect interpretation of the findings reported above. Indeed, ECs can secrete collagen IV (Kramer *et al*, 1984), which can be degraded by VEGF-induced MMPs (Coussens and Werb, 1996;

Girolamo *et al*, 2004). Both collagen and VEGF might serve as guidance cues for cell locomotion. We therefore hypothesized that (1) HUVEC cells secrete components of ECM, including collagen, in the context of our experiment, that is, on the scale of one or two cells; (2) secreted ECM can serve as a guidance cue allowing, in particular, retracing by cells of significant segments of their trajectories; (3) VEGF might modify the guidance effects of ECM by serving as chemoattractant and by modifying cell sensitivity to ECM, for example, through affecting MMP secretion. The last hypothesis is consistent with the effects of VEGF signalling inhibition on the movement of single HUVEC cells and HUVEC cells pairs described above. The lack of significant effect of VEGF inhibition on cell movement in A459–HUVEC pairs might reflect attractive interaction between these cells that is independent of VEGF.

HUVEC cells can follow secreted collagen trails

To test the above-mentioned hypotheses, we examined the deposition of collagen IV on the cell substratum, the effect of blocking collagen IV by an anti-collagen IV antibody and the corresponding change in the average cell speed over time. In-device staining of the cell migration surface with anti-collagen IV antibody after a live-cell imaging session revealed collagen IV 'footprints' (Supplementary Figure 6). Stacked epifluorescent images of HUVEC cells were also obtained by overlaying images over the course of the 17 h experiment. The outline of the collagen footprints displayed good correspondence to the overlaid cell positions for all cell combinations in the starvation medium. This result suggests that collagen IV is indeed secreted by the cells over the duration of experiment.

We next tested the ability of anti-collagen IV antibody to block interactions between cells and ECM. We exploited an advantage of this experimental design, that is, the ability to reseed cells for the follow-up experiment directly onto the collagen footprints left by cells from the first experiment stained with anti-collagen IV antibody. We found that HUVECs adhered to footprints at a much lower frequency and were not able to fully spread, indicating that antibody had indeed blocked the potential adhesion sites on both collagen IV and fibronectin (Supplementary Movie 4).

We then used the blocking property of the anti-collagen antibody to further investigate the influence of collagen IV on cell motility. We continuously supplied 0.125 μg/ml of the antibody in the culture medium during the cell patterning and culturing experiments. The resultant cell trajectories were, for the most part, longer and more persistent compared with the corresponding experiments without the antibody treatment, but displayed less frequent and extensive trajectory retracing periods (Figure 4). The directionality of cell movement increased from 2.2 ± 0.27 to 5.6 ± 1.1 for single HUVECs (P=0.03, standard t-test) and from 2.5 ± 0.66 to 5.3 ± 1.2 for cells in HUVEC pairs (P=0.05, standard t-test). The resultant cell separation was more extensive, which was strikingly reiterated by the rapid increase of the average inter-cell distance in HUVEC cell pairs after approximately 6 h of incubation in cell starvation medium complemented with the antibody. This was markedly distinct from a much more moderate increase in the average cell separation in pure starvation medium or the starvation medium complemented with the VEGF inhibitor. Longer, more persistent trajectories also led to an increase in the directionality of cell movement in the presence of the antibody for single HUVEC cells and HUVEC cell pairs, although directionality was not significantly altered for A549–HUVEC pairs. These results were consistent with a gradual deposition of collagen IV by migrating cells followed by binding of anti-collagen antibody, which in turn shielded the potential cell adhesion sites (both on collagen IV and other ECM components) decreasing the ability of cells to retrace their trajectories.

Biphasic cell speed variation with time

We next examined changes in the average cell speed over the duration of the experiment as a function of time and the incubation conditions. We found that in the complete medium, cells in all combinations have reached the maximum speed values (ranging from 0.6 μm/min for A549–HUVEC to 1 μm/min for cells in HUVEC–HUVEC pairs) between 8 and 10 h, with a subsequent moderate but not statistically significant slow-down (Figure 5). Cell behaviour under starvation conditions was very similar, with two exceptions: (a) the maximum speeds were markedly lower (ranging from 0.3 μm/min for HUVEC–HUVEC to 0.6 μm/min for A549–HUVEC cell pairs); (b) opposite of what was observed in the complete medium, the cells in A549–HUVEC cell pairs and single HUVECs moved significantly faster than cells in HUVEC cell pairs (Figure 5). In a striking contrast to cell behaviour in these two media, in the starvation medium complemented with the VEGF inhibitor, cells underwent a dramatic slow-down of cell movement at 4–6 h in all cell combinations, to speeds of 0.1–0.2 μm/min. The speed decrease was not due to deteriorating cell health, as the vast majority (over 95%) of cells were determined to be viable both by normal cell morphology and results of live/dead assay (data not shown). This suggests that VEGF inhibition does not potentiate cell death during the time course of our experiments, thus affecting cell speed more directly.

The deceleration observed at later stages of cell movement in all media types was consistent with the hypothesized increase in secretion of ECM components, including collagen IV, as cell speed is known to depend biphasically on the concentration of extracellular matrix proteins, decreasing at higher ECM densities after reaching the optimal speed (Palecek *et al*, 1997). To further verify this, we reseeded HUVECs into a chip preused for a 17 h experiment in a complete medium, which was then stripped of the cells. Unlike that in the experiment shown in Supplementary Movie 4 and described above, we did not stain collagen IV footprints with the anti-collagen antibody. Thus cell adhesion and spreading were not compromised, allowing us to detect and analyse cell movements. We observed, in sharp contrast to the results shown in Figure 5A, that the average cell speed started to decrease from the very beginning of cell movement, ultimately reaching a very low value of 0.1–0.2 μm/min (Supplementary Figure 7). This observation further confirmed that cells responded to absolute collagen concentration by altering their speed: the speed can increase to an optimal level and then decrease, as the collagen concentration increases.

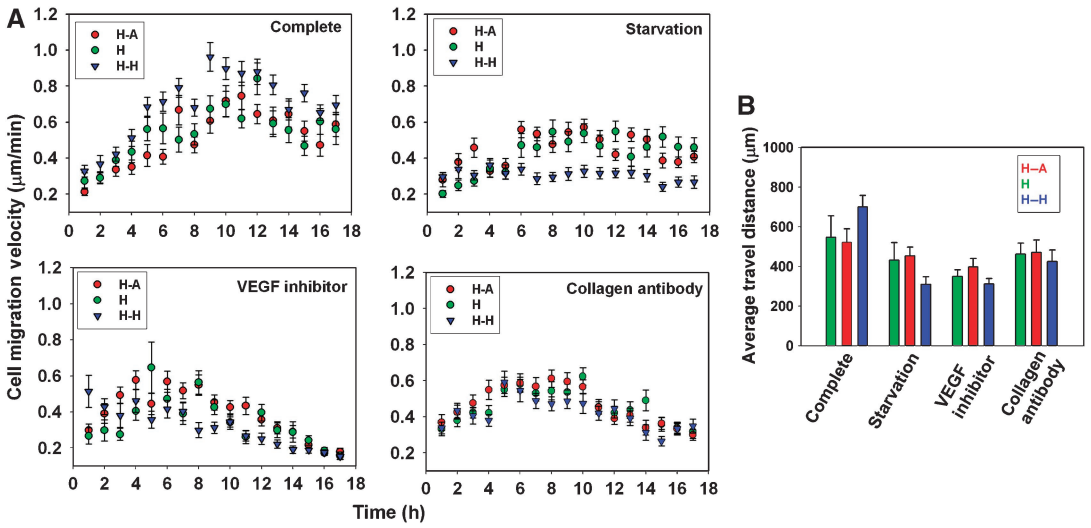

Figure 5 HUVEC migration speed. (**A**) Migration speed of HUVECs during a 17 h time course for cells incubated with indicated media. Each point represents the average of the speed values for all cells of a specific type at the indicated conditions binned within 1 h time intervals. (**B**) The average cell migration distance from the initial location during the same time course for HUVECs in HUVEC–A549 pairs (red), single HUVECs (green), HUVECs in HUVEC–HUVEC pairs (blue). Error bars represent s.e.m. (n=7–12 cells in each case with 6 speed measurements per hour binned, yielding a sample size of 42–72 for each plotted data point).

The relatively stronger deceleration of cell movement in the presence of VEGF inhibitor further suggested that collagen IV accumulated faster under this condition, possibly because of lower degradation rate (e.g., due to low MMP secretion). This further suggested the way VEGF might decrease ECM-mediated guidance by promoting ECM (collagen in particular) degradation, and thus decreasing availability of cell-secreted ECM as a cue. The same effect would be expected from other means of decreasing collagen availability. For instance, in the presence of the anti-collagen IV antibody, a gradual blockage of cell adhesion sites on the substratum might occur, as suggested above, leading to less efficient traction forces and thus decreasing average cell speed. Indeed, in the presence of the anti-collagen antibody, the average cell speed also significantly decreased at later stages of cell movement (Figure 5).

Agent-based model predicting vascular bed patterning

Taken together, the experimental observations described above suggested a set of rules governing the coordinated movement of HUVECs, either as isolated cells or within cell pairs:

- HUVECs secrete appreciable amounts of ECM components, including collagen, on the scale of one or two cells;
- secreted ECM components can serve as a guidance cue on the same scale allowing, in particular, for retracing by cells of significant segments of their own trajectories;
- cells respond to absolute collagen concentration by altering their speed: the speed can increase to an optimal level and then decrease, as the collagen concentration progressively increases;
- HUVECs secrete VEGF, which modifies the guidance effects of ECM, possibly by promoting ECM degradation;
- HUVECs respond to the absolute VEGF concentration by progressively losing their sensitivity to ECM (e.g., collagen) guidance; as the concentration of VEGF increases, cell movement along collagen tracks left by other cells becomes more erratic.

Agent-based modelling can allow one to test whether a set of rules describing responses of individual agents (e.g., representing living cells) might generate complex emergent properties when many agents are allowed to interact. It is generally observed that even few simple rules might lead to complex interactions by the agents, leading to complex agent population behaviour. Therefore, we explored whether an agent-based model incorporating the simple rules formulated above could reproduce some aspects of self-organization of ECs during angiogenesis, including branched geometry frequently associated with a vascular tree. Indeed, with one additional widely accepted assumption—ECs respond to VEGF gradient by chemotactically moving towards the higher concentration (Lamalice *et al*, 2007; Barkefors *et al*, 2008)—our simulation succeeded in recapitulating formation of a continuous and progressively branched vascular sprout (Figure 6 and Supplementary Movie 5). In the agent-based model, cells derived from a source representing existing blood vessels participating in angiogenesis were assumed to dissociate from the blood vessel and move in response to VEGF and ECM cues, as assumed above, as well as undergo periodic cell division. The tumour cells were not described explicitly, as we wanted to model mass or relatively passive tumour cells, and thus represented their effect by a simulated VEGF gradient. As model cells progressed through the available spatial computational domain, they deposited collagen providing new ECM-based cues for themselves and cells in their neighbourhoods. The collagen trails left behind by the leading cells were sufficient to direct the movement of the follower cells as they approached the VEGF source until arrival in the area where the ambient VEGF concentration substantially reduced their sensitivity to ECM. In this area, stochastic fluctuations in the directional guidance of cells by

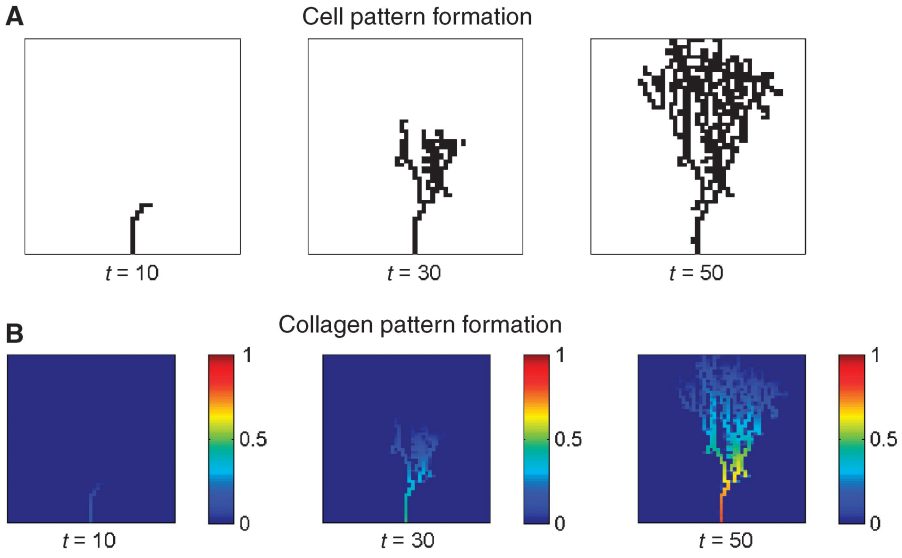

Figure 6 Time evolution of simulated cell and collagen patterns on the basis of the rules inferred from endothelial cell–cell interactions investigated in this study. Simulations were carried out for 50 time steps according to the rules specified in the Materials and methods section. Collagen and VEGF sensitivity factors were set at a=100 and b=150, respectively. (**A**) Cell patterns. (**B**) Collagen patterns shown for scaled concentrations.

the ECM trails increased, leading to increased formation of new branches, a characteristic common to developing blood vessels during angiogenesis (Figure 6A) As cells travelled along the existing ECM trails, the pattern of ECM became reinforced and closely resembled the ultimate cellular pattern (Figure 6B).

Overall, the simulations described above show that the application of simple rules derived from the analysis of individual cells and cell pairs can lead to more complex and organized structures on the scale of multiple cells. One of the more surprising results of the experimental analysis has been the ability of single cells to secrete, over a rather limited time course, enough of collagen IV to control their own trajectories and the trajectories of the neighbouring cells. We therefore studied how the results of the simulations would change if either the assumed rate of ECM (e.g., collagen) secretion or cell sensitivity to ECM were varied. We found that the predicted vascular patterns were very sensitive to both these parameters resulting either in a severe decrease in branching and thus tissue vascularization, if the values were high, or in a dramatic increase in branching and progressive vessel structure disorganization, when the parameter values were low (Figure 7). These results imply that guidance by collagen or other ECM components can be defined by optimal values of collagen secretion and by collagen sensitivity of individual cells, and that these parameters can be used to alter the structure of developing vascular bed, for example, through VEGF signalling.

Discussion

In this report, we describe a novel assay system combining the advantages of DEP and microfluidics for the analysis of interactions in homotypic and heterotypic cell pairs. The device allows one to initially pattern arrays of cell pairs and single cells with precisely controlled distances between the cells both within a pair and between cell pairs. This ensures a better controlled uncoupling of the influences of the immediate cell neighbour from more general cell population effects. Importantly, owing to diffusion-based medium exchange in the area of cell residence within the device, the distributions of the diffusible signalling molecules secreted by the cells are expected to be minimally perturbed, enabling analysis of long-term cell interaction behaviour, while ensuring continuous supply of fresh nutrients and other essential medium components. The ability to obtain different combinations of cells, including single cells and homo- and heterotypic cell pairs, makes the comparison of different types of cell interactions internally controlled.

The design of the DEP component of the device is based on a planer electrode array, and is more easily fabricated compared with previous positive DEP devices (Gray *et al*, 2004). Fabricating the electrode array as a transparent ITO layer coated on a glass substrate allowed us to avoid blocking the view of live cells, and thus permitted using conventional inverted microscope; thus all cell patterning, stimulation and monitoring of live cell response could be performed in the same experiment, in the same device. The diffusion-based microfluidic channel network, precisely aligned with the electrode arrays, has the advantage of minimal perturbation of cell position due to negligible active flow through the cell containing area, as demonstrated previously (Paliwal *et al*, 2007). In combination, the DEP and microfluidic flow control capabilities endowed us with the capacity to analyse cell movements over extended periods of time from precisely defined initial positions. The new experimental capabilities afforded by this device can facilitate studies aimed at elucidating the details of autocrine, paracrine and juxtacrine cell–cell communications occurring over long-term cell culturing within a controlled cell microenvironment. These

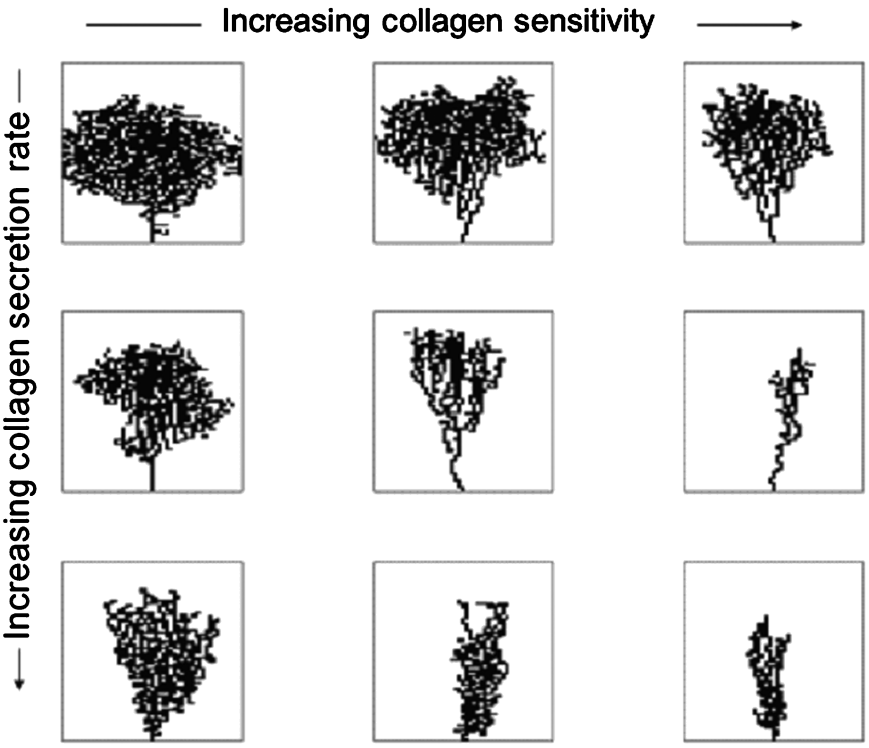

Figure 7 Influence of simulation parameters on cell pattern formation. Sensitivity to collagen was varied from left to right as a=25, 100 and 200. Collagen secretion rate was varied from top to bottom as 0.005, 0.02 and 0.08.

properties should make this device useful for investigation of a multitude of problems in signal transduction and cell–cell communication.

Using this device, we analysed the motion of single cancer and ECs as well as pairs of these cells, under a range of conditions. Our findings suggest that ECs can be strongly affected by secreted ECM components and VEGF, both of which can influence cell migration. Secreted, substratum-adherent collagen IV and, possibly, other secreted ECM components appear to endow HUVECs with positional memory, allowing them to retrace portions of their trajectories or follow the trajectories of other HUVECs, an effect masked by VEGF under starvation conditions. In addition to the inhibition of VEGF, presence of a neighbouring cancer cell in a cell pair appeared to increase the positional memory in EC movements, in a VEGF-independent manner. VEGF inhibition also led to coupling of trajectories of two neighbouring ECs, with their movements becoming coordinated and aligned, often (and on average) evolving into an oscillation-like pattern, in which cells periodically approached one another. Alternatively, cells often followed each other, occasionally with three or more cells following each other in a tandem formation.

The biphasic change in the average cell speed over time suggests that the secreted matrix can also affect the rate of cell locomotion. Indeed, the biphasic nature of the effect of the ECM density on cell speed has long been known (Palecek *et al*, 1997), thus progressive accumulation of the matrix components might differentially influence cells over time. The decrease in speed was much more dramatic in the presence of the VEGF inhibitor, although the maximum speed achieved under this condition and the time at which the maximum speed was achieved were similar to those found in the absence of the drug. This suggests that the effect of VEGF is more pronounced at later time points (4 h into the experiment), possibly because a prolonged period of time is necessary for VEGF accumulation within the cell residence chambers. Indeed, the estimated approximate time of accumulation of a diffusive substance similar to VEGF ($D \sim 10^{-7}\,cm^2/s$) over the characteristic distance of 100 μm is approximately 3–5 h (Squires and Quake, 2005). Alternatively, if the effect of VEGF is indirect, for example, due to modulation of the effect of collagen, the delayed effect of VEGF inhibition could indicate the need for a gradual collagen accumulation. Consistent with this possibility, addition of an anti-collagen antibody led to a substantial reduction in the average cell speed at later stages of cell movement, probably due to shielding of both the collagen IV binding sites and the bindings sites of other ECM components by the antibody molecules binding to the gradually accumulating newly secreted collagen IV. This experiment suggested that the effects of collagen IV accumulation are more prominent at later time points (5–7 h into the experiment), consistent with a rapid increase in the average cell–cell distance in HUVEC pairs observed at this time in the presence of the antibody (Figure 4).

Vascular endothelial growth factor shapes developing vascular networks through a variety of mechanisms, including those regulating cell proliferation and migration. EC migration can also be affected by haptotaxis in complex fields of ECM components. The interactions between these two prominent

morphogenic cues are still not fully understood. Our results suggest that, on the level of one or a few ECs, VEGF inhibition can increase the guidance function of the secreted ECM components and thus can enhance the auto- and cross-coordination of cell movement that might be crucial for forming well-organized vascular networks.

The agent-based model presented in this study further supported the predictions of importance of ECM-based cell guidance. The simulation rules that governed the behaviour of cells were limited to chemotaxis towards a VEGF source, hapotaxis in collagen (or possibly other ECM components), secretion of collagen and proliferation. Unlike most existing agent-based models of angiogenesis (for example, the models described in Introduction), neither specific rules that might constrain branch formation nor predefined heterogeneities in the ECM were required for the evolution of vascular branching. Of course, the presented model neglects many other important cell–cell and cell–matrix interactions, but it is all the more striking that a very simple set of rules is sufficient to generate a wealth of patterns bearing similarity to the geometric complexities of the angiogenic vascular beds. Overall, our model further illustrates that the factors that influence the interaction of cells at the level of a cell pair, such as the secretion of collagen IV, shown here experimentally, can provide insight into the mechanism for the formation of more complex multicellular structures. In a more general sense, use of such models might be a convenient way to scale up the observations from limited numbers of cells into a predicted behaviour of multicellular ensembles and tissues, determining in the processes whether further assumptions describing multicell community effects might be needed to elucidate tissue behaviour, or whether a fully reductionist approach can be used.

It may be interesting to contrast our findings with the recent observations that the Notch pathway activation in ECs, leading to inhibition of VEGFR, is essential for correct formation of vascular microbeds, in part through a decrease in excessive vessel branching (Noguera-Troise *et al*, 2006; Ridgway *et al*, 2006). Our results suggest that the Notch-mediated decrease in VEGF activity may increase the ECM-mediated coordination of cell movement and thus might decrease excessive and inappropriate formation of new sprouts.

One of the more surprising findings of our analysis was that the effects of the cancer cells in pairs with ECs on EC speed and trajectory directionality were minor and mostly statistically insignificant. This was counter to our initial expectations that cancer cells, by virtue of secreting chemoattractant growth factors, such as VEGF, would significantly affect the movement of the neighbouring ECs. We believe that our results imply that the attractive effect of cancer cells (or more specifically alveolar basal epithelial carcinoma cells used in the study) might require collective rather than a single cell influence on stromal cells (e.g., the cells of endothelium). Alternatively, further alteration of the cell medium might enhance the cancer cell effects, that is, through the induction of local hypoxia.

The results presented above argue that the methodology allowing efficient patterning of homotypic and heterotypic cell pairs as well as single cells might help unravel interactions occurring in more complex cell ensembles, including animal and human tissues. This scale of analysis can reveal whether the interactions occurring on this smallest scale can be sufficient to explain collective cell behaviour, or further assumptions are needed to reflect the cumulative effect of cell numbers. We foresee then that the methodology proposed here will find a wide use in the hands of researchers interested in hierarchical cell–cell interactions underlying complex tissues formation in both health and disease.

Materials and methods

Cell culture and reagents

Immortalized human umbilical vein cells (a generous gift from Dr Folkman, Massachusetts General Hospital) and described by Freedman and Folkman (2004) were cultured in EGM-2 medium (basal medium plus a supplemental kit from Cambrex, USA) supplemented with 5% heat-inhibited FBS. According to the vendor, VEGF concentration in this medium is between 1 and 10 ng/ml. A549 human lung cancer cells (ATCC, USA) were cultured in F12/HAM (Gibco) supplemented with 10% FBS and 1% penicillin–streptomycin solution (Gibco). Both cell lines were cultured at 37°C and in the presence of humidified 5% CO_2/air atmosphere. VEGF inhibitor CBO-P11 was purchased from CalBioChem (EMD Biosciences Inc., USA). VEGFR 2 antibody (MAB3572) was purchased from R&D Systems. The details of cell coculture experiments can be found in the text. Live/dead cell assay kit (L3224) was purchased from Invitrogen (USA).

Device design and fabrication

The fabrication procedure is shown in Supplementary Figure 1. ITO-coated 0.7 mm glass slides (Structure Probe Inc.) were used to form an ITO transparent electrode array on glass substrate. According to the information obtained from the vendor, the thickness of the ITO layer is 120–160 nm, with a total resistance of 8–10 Ohms/cm^2. The transmittance was greater then 83%. The glass slides were cleansed with acetone and IPA and then coated with S1813-positive photoresist (Shipley, USA). A high-resolution—20 000 d.p.i.—transparency mask (CAD/Art Services Inc.) with the design of the triangular electrode array (Figure 1A) was used for UV patterning. After development of the photoresist layer, the ITO layer was etched by Tin oxide etchant TE100 (Transene Company Inc.) for about 10 min. Four electrode columns were connected to two base bars for external electric connection (Figure 1A). The triangular electrode design was chosen after simulation with FEMLAB for several different structures and was found that this design can effectively form field maxima around the electrode tips (Figure 1B), so as to capture no more than a single cell on each tip using positive DEP force.

The microfluidic channel network was based on the design previously described by Paliwal *et al* (2007), whose performance was further simulated using FEMLAB. Simulations confirmed that culture media are expected to flow through the side channels, and chemicals contained therein diffuse into the test channels connecting the side channels (Supplementary Figure 2). Shear stress on the cells positioned in the test channels was minimized. The microfluidic network was fabricated by casting PDMS onto a SU8 mould. SU8-2025 (Microchem Inc.) was spin-coated on a silicon wafer at 1750 r.p.m. to get a thickness of about 50 μm. The SU-8 layer was then patterned with another transparency mask and developed to form the microchannel network mold (Supplementary Figure 1). The mold with PDMS was baked at 80°C for 1.5 h. PDMS was then peeled off from the mold, cutted, drilled with inlet/outlet holes and finally bonded with the glass slide with the electrode array. The device was baked at 85°C overnight. Figure 1A shows the final device.

The gaps between electrode tips were varied, but always less than 40μm. This distance was chosen so that cells in a pair captured by electrodes facing each other would form a contact after fully spreading, and the initial distance between cells in a pair could be taken to be zero. There were 240 electrodes total in four channels (60 electrodes per channel). The fluidic channels for cell culturing were 0.8 mm wide and 4 mm long.

Device operation

Before cells were introduced into the chip, the substrate was coated with 100 μg/ml fibronectin in 0.01 M HCl for 30 min. Solutions of gelatin (0.1%), collagen (10 and 100 μg/ml) and fibronectin (10 and 100 μg/ml) at different concentrations were tested as coating materials. It was found that 100 μg/ml fibronectin was optimal for cell attachment on the substrate (data not shown). The channels were then washed with solution made of 90% DEP medium (0.3 Osm sucrose solution with 1% FBS and 20 mM HEPES, pH 7.4) and 10% HUVEC culture medium. Cells were detached from cell-culture flasks and resuspended in 200 μl of DEP medium at the density of 2.0×10^5 cells/ml (Gray *et al*, 2004), then introduced into the device through the cell-seeding ports (see Figure 1A). After the cells entered the channels, an AC electrical potential of 4 Vpp at 3 MHz generated by a function generator (33220A, Agilent) was applied to the electrodes. The frequency of 3 MHz was chosen to achieve the value of the polarization factor maximizing the positive DEP force (Gascoyne *et al*, 1997). The flow of this medium continued until every electrode tip captured one or several cells. Then the flow was reversed and the solution was changed to 90% DEP medium/10% culturing medium to wash away weakly adhering cells, in most cases leaving no more than one cell per electrode tip. A concentration of 10% culturing medium was found not to dramatically change the properties of the DEP, but to nevertheless allow the cells to attach on the surface faster after patterning. The flow and electrical supply were then stopped and cells were allowed to attach in this solution for about 40 min at 37°C. Cells were then continuously perfused with the culture medium through the feeding ports (see Figure 1A) and cultured at 37°C and in the presence of humidified 5% CO_2/air atmosphere on the stage of a Zeiss inverted microscope (Axiovert 200 M). Phase-contrast and/or fluorescence images of live cells were taken using a cascade CCD camera (Photometrics) attached to the microscope with an objective of ×10 or ×20 (NA=0.4) (Supplementary Movie 2). In all experiments, cell images were visually examined before analysis, and occasional instances of cells displaying morphology changes characteristic of apoptosis (alteration of morphology, shedding of plasma membrane and initiation of disintegration) were excluded from analysis.

In-chip fluorescent immunostaining

Rabbit polyclonal anti-collagen IV antibody ab21295 and secondary goat anti-rabbit antibody Alexa Fluor 594 were purchased from Abcam and Molecule Probes (Invitrogen, USA), respectively. For in-chip immunostaining of the cell-secreted collagen-IV, trypsin was first flowed into the chip to remove cells. After blocking with 10% goat serum/PBS, the device was incubated with 1:100 primary anti-collagen IV antibody followed by 1:200 secondary antibody.

Cell trajectories and their directionalities

To obtain cell trajectories, HUVEC cells in fluorescent image sequence were segmented using Matlab functions (version 7.2, MathWorks). Centroids of the segmented cells were recorded. A trajectory follows the movement of the centroid in an image sequence. Cell trajectories were assembled randomly with respect to each other but preserving their orientation with respect to electrode geometry in Figures 2–4 The envelopes of cell trajectories were fitted with the ellipse formula: $(x/a)^2 + (y/b)^2 = 1$ in appropriate coordinates, and the resultant ratio of the major (a) to minor (b) axes was used as the measure of directionality of the cell path. The directionality metric thus corresponds to the eccentricity of the ellipse fitting the data. Trajectory data were imported into Matlab and following standard functions were used: objects.MajorAxisLength and objects.MinorAxisLength. Cell speed was determined by dividing the travel distance of centroid between two time points over the corresponding time interval and averaged over an hour.

Agent-based model of EC migration and vascular bed patterning

The agent-based model presented here is constructed on a fixed (NxN) two-dimensional square grid, throughout which cells are modelled as discrete entities. Each cell occupies a single node within the grid. Interactions between cells and their environment are described by considering a four-section neighbourhood consisting of adjacent northern, southern, eastern and western nodes (Supplementary Figure 2A). Cells enter the computational domain from the centre of the lower portion of the grid and are exposed to a linear gradient of VEGF (Supplementary Figure 2B). The concentrations of collagen and VEGF are scaled from 0 to 1. Cell movement and behaviour is based on a biased random walk according to the following rules inferred from the experimental results, as discussed in the text:

1. The decision whether a cell moves or remains in the same location during each time step is dependent on the local concentration of collagen (or, possibly, other ECM components). The probability of movement is set such that either very low or very high concentrations of collagen result in a lower chance of movement. Intermediate collagen concentrations result in the highest probability of cell movement. The corresponding function is shown in Supplementary Figure 3.
2. Cells can move in one of four different directions (north, south, east and west). Each cell is biased to move towards the direction of greatest collagen concentration within its neighbourhood. In addition, cells are also driven to move up the imposed VEGF gradient. A cell's sensitivity to VEGF is described using a binomial function (F_v) with an integer weighting factor b (equation (1)). Sensitivity to collagen was described by a similar binomial function (F_c) with the exception that the weighting factor a was dependent on VEGF (equation (2)). Sensitivity to guidance cues from collagen therefore decreased as cells entered areas of higher VEGF concentration. The probability of moving in any given direction (P^i) is therefore a function of both collagen (C_c) and VEGF (C_v) concentrations and is given by the following equations:

$$F_v = (1 + C_v)^b \tag{1}$$

$$F_c = (1 + C_c)^a \tag{2}$$

where a=(c/(1 + d*C_v)) and c and d are addition weighting factors.

$$P^i = \frac{F_c^i F_v^i}{\sum_{i=1}^{4} F_c^i F_v^i} \tag{3}$$

3. Only one cell can occupy one grid node at any given time.
4. Cells secrete a fixed amount of collagen at each time step, which can act as a guidance cue for the secreting cell or other cells. The concentration of collagen at nodes occupied with cells therefore increases at a rate proportional to the frequency at which the node is occupied. The collagen secreted by cells decays throughout the simulation at a rate five times slower than the rate of its secretion by cells.
5. Cell division is contact-inhibited such that only cells with one neighbour are allowed to divide.

All simulations were performed using Matlab (version 7.2, MathWorks).

Supplementary information

Supplementary information is available at the *Molecular Systems Biology* website (www.nature.com/msb).

Acknowledgements

This work was supported by the seed grant from the Institute for Cell Engineering at the Johns Hopkins Medical Institutions. We are also grateful for helpful discussions with Dr Rhoda Alani, Dr Gregg Semenza, Raymond Cheong and other members of Levchenko lab.

Conflict of interest

The authors declare that they have no conflict of interest.

References

Adams RH, Alitalo K (2007) Molecular regulation of angiogenesis and lymphangiogenesis. *Nat Rev Mol Cell Biol* **8:** 464–478

Anderson AR, Chaplain MA (1998) Continuous and discrete mathematical models of tumor-induced angiogenesis. *Bull Math Biol* **60:** 857–899

Barkefors I, Le Jan S, Jakobsson L, Hejll E, Carlson G, Johansson H, Jarvius J, Park JW, Li Jeon N, Kreuger J (2008) Endothelial cell migration in stable gradients of vascular endothelial growth factor A and fibroblast growth factor 2: effects on chemotaxis and chemokinesis. *J Biol Chem* **283:** 13905–13912

Bauer AL, Jackson TL, Jiang Y (2007) A cell-based model exhibiting branching and anastomosis during tumor-induced angiogenesis. *Biophys J* **92:** 3105–3121

Chen C, Mrksich M, Huang S, Whitesides G, Ingber D (1997) Geometric control of cell life and death. *Science* **276:** 1425–1428

Coussens L, Werb Z (1996) Matrix metalloproteinases and the development of cancer. *Chem Biol* **3:** 895–904

Di Talia S, Gamba A, Lamberti F, Serini G (2006) Role of repulsive factors in vascularization dynamics. *Phys Rev E* **73:** 041917

El-Ali J, Sorger PK, Jensen KF (2006) Cells on chips. *Nature* **442:** 403–411

Ferrara N (2004) Vascular endothelial growth factor as a target for anticancer therapy. *Oncologist* **9** (Suppl 1)**:** 2–10

Folkman J (2007) Angiogenesis: an organizing principle for drug discovery? *Nat Rev Drug Discov* **6:** 273–286

Freedman D, Folkman J (2004) Maintenance of G1 checkpoint controls in telomerase-immortalized endothelial cells. *Cell cycle* **3:** 811–816

Gamba A, Ambrosi D, Coniglio A, de Candia A, Di Talia S, Giraudo E, Serini G, Preziosi L, Bussolino F (2003) Percolation, morphogenesis, and burgers dynamics in blood vessels formation. *Phys Rev Lett* **90:** 118101

Gascoyne P, Wang X, Huang Y, Becker F (1997) Dielectrophoretic separation of cancer cells from blood. *IEEE Trans Ind Appl* **33:** 670–678

Girolamo F, Virgintino D, Errede M, Capobianco C, Bernardini N, Bertossi M, Roncali L (2004) Involvement of metalloprotease-2 in the development of human brain microvessels. *Histochem Cell Biol* **122:** 261–270

Glazier JA, Graner F (1993) Simulation of the differential adhesion driven rearrangement of biological cells. *Phys Rev E Stat Phys Plasmas Fluids Relat Interdiscip Topics* **47:** 2128–2154

Gray D, Tan J, Voldman J, Chen C (2004) Dielectrophoretic registration of living cells to a microelectrode array. *Biosens Bioelectron* **19:** 1765–1774

Hanahan D, Weinberg R (2000) The hallmarks of cancer. *Cell* **100:** 57–70

Herbst R, Sandler A (2004) Non-small cell lung cancer and antiangiogenic therapy: what can be expected of bevacizumab? *Oncologist* **9** (Suppl 1)**:** 19–26

Irimia D, Karlsson JOM (2003) Development of cell patterning technique using poly(ethylene glycol) disilane. *Biomed Microdev* **5:** 185–194

Kane R, Takayama S, Ostuni E, Ingber D, Whitesides G (1999) Patterning proteins and cells using soft lithography. *Biomaterials* **20:** 2363–2376

Khademhosseini A, Suh K, Jon S, Eng G, Yeh J, Chen G, Langer R (2004) A soft lithographic approach to fabricate patterned microfluidic channels. *Anal Chem* **76:** 3675–3681

Kramer R, Bensch K, Davison P, Karasek M (1984) Basal lamina formation by cultured microvascular endothelial cells. *J Cell Biol* **99:** 692–698

Lamalice L, Le Boeuf F, Huot J (2007) Endothelial cell migration during angiogenesis. *Circ Res* **100:** 782–794

Lee S, Chen TT, Barber CL, Jordan MC, Murdock J, Desai S, Ferrara N, Nagy A, Roos KP, Iruela-Arispe ML (2007) Autocrine VEGF signaling is required for vascular homeostasis. *Cell* **130:** 691–703

Lin R, Ho C, Liu C, Chang H (2006) Dielectrophoresis based-cell patterning for tissue engineering. *Biotechnol J* **1:** 949–957

Lucchetta E, Lee J, Fu L, Patel N, Ismagilov R (2005) Dynamics of *Drosophila* embryonic patterning network perturbed in space and time using microfluidics. *Nature* **434:** 1134–1138

Mantzaris NV, Webb S, Othmer HG (2004) Mathematical modeling of tumor-induced angiogenesis. *J Math Biol* **49:** 111–187

Matsumoto T, Claesson-Welsh L (2001) VEGF receptor signal transduction. *Sci STKE* **112** (RE21)**:** 1–17

Melin J, Quake SR (2007) Microfluidic large-scale integration: the evolution of design rules for biological automation. *Annu Rev Biophys Biomol Struct* **36:** 213–231

Merks RMH, Brodsky SV, Goligorksy MS, Newman SA, Glazier JA (2006) Cell elongation is key to *in silico* replication of *in vitro* vasculogenesis and subsequent remodeling. *Dev Biol* **289:** 44–54

Merks RMH, Glazier JA (2006) Dynamic mechanisms of blood vessel growth. *Nonlinearity* **19:** C1–C10

Nelson C, Chen C (2002) Cell–cell signaling by direct contact increases cell proliferation via a PI3K-dependent signal. *FEBS Lett* **514:** 238–242

Nelson C, Chen C (2003) VE-cadherin simultaneously stimulates and inhibits cell proliferation by altering cytoskeletal structure and tension. *J Cell Sci* **116** (Part 17)**:** 3571–3581

Noguera-Troise I, Daly C, Papadopoulos NJ, Coetzee S, Boland P, Gale NW, Lin HC, Yancopoulos GD, Thurston G (2006) Blockade of Dll4 inhibits tumour growth by promoting non-productive angiogenesis. *Nature* **444:** 1032–1037

Palecek S, Loftus J, Ginsberg M, Lauffenburger D, Horwitz A (1997) Integrin-ligand binding properties govern cell migration speed through cell-substratum adhesiveness. *Nature* **385:** 537–540

Paliwal S, Iglesias PA, Campbell K, Hilioti Z, Groisman A, Levchenko A (2007) MAPK-mediated bimodal gene expression and adaptive gradient sensing in yeast. *Nature* **446:** 46–51

Ridgway J, Zhang G, Wu Y, Stawicki S, Liang W-C, Chanthery Y, Kowalski J, Watts RJ, Callahan C, Kasman I, Singh M, Chien M, Tan C, Hongo J-AS, de Sauvage F, Plowman G, Yan M (2006) Inhibition of Dll4 signalling inhibits tumour growth by deregulating angiogenesis. *Nature* **444:** 1083–1087

Serini G, Ambrosi D, Giraudo E, Gamba A, Preziosi L, Bussolino F (2003) Modeling the early stages of vascular network assembly. *EMBO J* **22:** 1771–1779

Shenberger JS, Zhang L, Powell RJ, Barchowsky A (2007) Hyperoxia enhances VEGF release from A549 cells via post-transcriptional processes. *Free Radic Biol Med* **43:** 844–852

Squires T, Quake S (2005) Microfluidics: fluid physics at the nanoliter scale. *Rev Modern Phys* **3:** 977–1026

Stokes CL, Lauffenburger DA (1991) Analysis of the roles of microvessel endothelial cell random motility and chemotaxis in angiogenesis. *J Theor Biol* **152:** 377–403

Suh K, Seong J, Khademhosseini A, Laibinis P, Langer R (2004) A simple soft lithographic route to fabrication of poly(ethylene glycol) microstructures for protein and cell patterning. *Biomaterials* **25:** 557–563

Takayama S, McDonald J, Ostuni E, Liang M, Kenis P, Ismagilov R, Whitesides G (1999) Patterning cells and their environments using multiple laminar fluid flows in capillary networks. *Proc Natl Acad Sci USA* **96:** 5545–5548

Veiseh M, Wickes B, Castner D, Zhang M (2004) Guided cell patterning on gold-silicon dioxide substrates by surface molecular engineering. *Biomaterials* **25:** 3315–3324

Voldman J, Braff R, Toner M, Gray M, Schmidt M (2001) Holding forces of single-particle dielectrophoretic traps. *Biophys J* **80:** 531–541

Wang X, Huang Y, Gascoyne P, Becker F (1997) Dielectrophoretic manipulating of particles. *IEEE Tran Ind Appl* **33:** 660–669

Weibel D, Whitesides G (2006) Applications of microfluidics in chemical biology. *Curr Opin Chem Biol* **10:** 584–591